Modeling multiple damage mechanisms via a multi-fiber multi-layer representative volume element (M²RVE)

GANESH SONI[1], RAMESH SINGH[2,*] , MIRA MITRA[3] and WENYI YAN[4]

[1] Department of Mechanical Engineering, IITB-Monash Research Academy, Mumbai, India
[2] Department of Mechanical Engineering, Indian Institute of Technology Bombay, Mumbai, India
[3] Department of Aerospace Engineering, Indian Institute of Technology Kharagpur, Kharagpur, India
[4] Department of Mechanical and Aerospace Engineering, Monash University, Melbourne, Australia
e-mail: rsingh@iitb.ac.in

Abstract. This paper is aimed at incorporating all possible micro-scale damage mechanisms, namely, fiber failure, matrix cracking, fiber-matrix debonding and delamination in multi-fiber multi-layer representative volume element (M²RVE) subjected to multi-axial loading. Different loading conditions have been selected to induce a particular or combined damage mechanism/s to study the damage evolution. The predicted constitutive material responses for tensile and in-plane shear loading by M²RVE are in reasonably good agreement with the experimental results. M²RVE then used for capturing all the microscale damage mechanisms even for complex multi-axial loading. The stress–strain responses have been effectively captured for different combinations of dominant damage mechanisms.

Keywords. Fiber damage; matrix damage; fiber-matrix debonding; delamination; mixed loading condition; multi-fiber multi-layer representative volume element.

1. Introduction

It is important to accurately predict the damage behavior for efficient and reliable designing of the composite structures. Typical macro-scale failure model makes use of Tsai-Hill, Hashin and Puck's damage criteria [1]. These models do not capture failure mechanisms at the fiber and matrix level. It is computationally expensive to carry out a full-scale microscopic analysis of the structure by explicitly modeling all the heterogeneities. In order to reduce computational cost and to study the micro-scale behavior of composites, multiscale methods are useful [2]. It has been established that multi-scale modeling can provide the desired accuracy in a computationally efficient manner. There are many multi-scale modeling methods like FE² [3], Sub-modeling method [4], Inter-scale theory [5], Micro-macro method [6]. Each approach has some advantages and some limitations and specific application area. For example, FE² method provides accurate results, however the method is computationally expensive and limited to use for 2D problems.

The most common multiscale modeling method is to utilize a representative volume element (RVE) to predict microscale damage mechanism using computational micromechanics through the homogenization process [7]. It

has been demonstrated that periodic boundary conditions provide a better prediction of the global material response as compared to displacement and traction boundary conditions [8]. Representative volume elements (RVEs) usually consist of either a single fiber or multiple fibers of the same diameter such that the volume fraction in the RVE is the same as that of the composite lamina [9–11]. Different loading conditions have been used to predict global material response and local failure like matrix damage and fiber-matrix debonding using a three-dimensional multiple fibers RVE [9, 10]. It is important to note that a single RVE can be used to predict the damage response of the composite lamina (ply). The effective properties can be used to predict the behavior of the laminate by considering the effect of stacking sequence. The work done using RVE is mostly limited to application of matrix damage and fiber matrix debonding [10–12]. Matrix damage has been captured by considering resin material as either elastic-plastic or visco-elastic in nature [9–11].

To simulate fiber failure, González and LLorca [12] have used randomly placed damageable (cohesive) elements along the fiber length. A random arrangement is provided to incorporate statistical variability of the properties of the fiber. Wang *et al* [13] have also used randomly placed damageable layers that have the same elastic properties as fiber material (except that they are damageable) along the fiber length. The basic limitation of the damageable layers

is that placement of the damageable layers along the length of the fibers affects the strength prediction results significantly. The point in the fiber at which damage is expected to initiate is already known. Also, initiation of the damage in damageable layers affects matrix damage evolution and fiber-matrix decohesion in the vicinity of the damage. Most of the studies in the literature using RVE consisting of two layers assume of perfect bonding between layers [12].

Cox *et al* [14] studied relationship between microstructure and evolution of damage events leading to failure using continuous fiber composites. A new augmented finite element method dealing with arbitrary systems of crack initiation in heterogeneous materials has been proposed. The work aims to provide light on stochastic nature of material microstructure on the composite's performance. Design parameters controlling damage behaviors of continuous fiber reinforced thermoplastic composites using micromechanics has been studies by Pulungan *et al* [15]. They have developed 3D RVE using periodic boundary conditions to minimize the edge effect. The RVE is subjected to transverse tensile loading and the simulation results are found to be in good agreement with experimental results for stiffness as well as for failure. Various micro scale failure modes including fiber–matrix debonding and matrix failure are studied in 2D RVEs extracted from the layer 90° in different cross-ply laminates by Madadi and Farrokhabadi [16]. To model failure cohesive zone model and extended finite element method (XFEM) has been used. Delamination initiation from the tips of matrix cracking has been captured using cohesive surfaces. Effects of shape and misalignment of fibers on the failure response of carbon fiber reinforced polymers has been studied by Ahmadian *et al* [17]. Tensile and compressive transverse loading has been used for all the studies. Ramdoum *et al* [18] performed interface debonding growth using the cohesive zone method. 3D RVE has been used to study the energy release rate (ERR) by the J integral method. It is attempted to study effect on failure due to angle of debonding between fibers and matrix material. Failure envelope of angle ply laminates has been estimated by Romanowicz M [19] using mesoscale finite element model. Damage by microcracking at the fiber–matrix interface and shear band formation in the matrix is incorporated in the numerical simulations.

Bargmann *et al* [20] reviews state of the representative techniques for composites. The paper covers study of more than 550 research papers and books on generation of 3D representative volume elements for heterogeneous material. Soni *et al* [21] has proposed multi-layer multi-fiber representative volume element which can capture fiber-matrix debonding and matrix cracking. However, the work did not incorporate fiber failure and the delamination between plies. Multifiber multilayer RVE has been used to capture stiffness response by Ullah *et al* [22]. Perfect bonding between the two layers has been considered. They have infact observed that difference between experimental results and simulation results can be attributed to inter-layer

perfect bonding. Very few studies in the literature have investigated delamination between laminate layers using computational micromechanics [23] and the interaction of delamination with other damage mechanisms has yet to be studied.

The focus of this paper is to use M^2RVE to capture all the damage mechanisms, namely, fiber failure, matrix damage, fiber-matrix and interlaminar decohesion for complex multi-axial loading. Fiber failure and matrix cracking are based on the maximum principal stress criterion and the multi-axial Mohr-Coulomb criterion, respectively. Fiber-matrix debonding and delamination between plies have been captured by introducing a cohesive layer in conjunction with standard traction separation law. It is known that the nature of damage evolution depends on the loading conditions. In-plane tensile loading primarily causes the tensile failure of fibers.

It is known that matrix failure and interface failure is dominating in case of shear loading as compared to transverse loading [9–12]. Moreover, an in-plane shear loading can be considered as combination of tensile and transverse loading from a theoretical standpoint. On this basis, testing in transverse direction is not considered in the current work. Instead a conservative loading i.e., in-plane shear loading is used. Out-of-plane tensile loading triggers delamination. Additionally, in order to study the evolution of different damage mechanisms simultaneously, a combination of loads which trigger different failure mechanisms has been considered. In simple words, current work covers combined micro level (fiber failure, matrix failure and fiber matrix debonding) as well as macro level (delamination) damage mechanisms using multi-layer representative volume element subjected to complex loading conditions.

2. Finite element modeling of M^2RVE

This section presents the finite element formulation a multi-fiber multi-layer representative volume element with multi-axial loading and periodic boundary conditions. The failure models for matrix failure, fiber-matrix debonding, fiber failure and delamination are also described.

2.1 *Geometrical configuration and the FE model*

Figure 1 illustrates a typical M^2RVE configuration for a [0/90]n laminate (n number of [0/90] laminates), as described in detail by Soni *et al* [21]. The M^2RVE can be used to model any symmetrical [0/90]n laminate because it uses periodic boundary conditions on all the faces. The model is comprised of two cubes which have multiple randomly distributed fibers of equal diameter placed perpendicular to each other. Circular fibers, 24 μm in diameter (used during manufacture of composite), have been distributed randomly via a fiber randomization algorithm in DIGIMAT FE® [24].
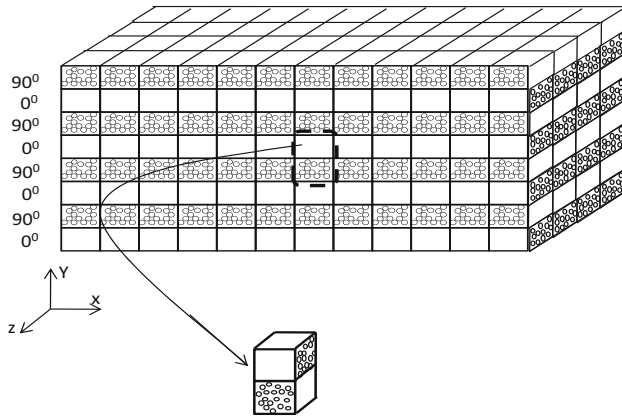
Figure 1. M^{2}RVE for [0/90]$_n$ laminate [21].

Adequate discretization has been ensured by placing each fiber at least 1 μm away from the other fiber. It has been ensured that the distance between the fiber surface and the M^{2}RVE edges is more than 0.5 μm to avoid distorted elements during meshing. The proposed microstructure is considered to have indefinite translation along all three axes, thus, fiber positions within the M^{2}RVE maintain periodicity. The fibers intersecting the RVE edges were split into two parts and copied to the opposite face to create a periodic microstructure as shown in figure 1.

The total number of fibers has been restricted in such a way that the volume fraction of fibers in the matrix is ~28%. The experimental spacemen were created using hand lay-up techniques, therefore, there was no control over the volume fraction obtained is on slightly lower side. The stress-strain response of the M^{2}RVE has been investigated using finite element method (FEM). The M^{2}RVE (matrix and fibers) has been meshed using a four-node linear tetrahedral (C3D4) elements in ABAQUS Standard® [4]. A modified quadratic 10-node tetrahedral (C3D10M) elements were also evaluated but did not yield any appreciable change in results. Consequently, computationally efficient C3D4 elements have been used in this study.

Cohesive elements have been included between each fiber and matrix material to capture fiber-matrix debonding. A thin layer of COH3D6 cohesive elements have been provided between 0° lamina cube and 90° lamina cube to capture possible delamination. Note that the size of the M^{2}RVE must be large enough to ensure that the average properties do not depend on either the size and or the location of the reinforcement phase, and their spatial distribution. In the previous study by Soni *et al* [21], a parametric study was performed to determine the size of each cube in M^{2}RVE. In that study, the edge length of each M^{2}RVE was varied between 0.1 mm and 0.5 mm and global stress and strain response were found to be insensitive to the size of the RVE. Therefore, a cube of 0.1 mm edge size has been used in this study.

2.2 *Boundary conditions*

Figure 2 shows a schematic 2D unit cell under macro strain with periodic boundary conditions.
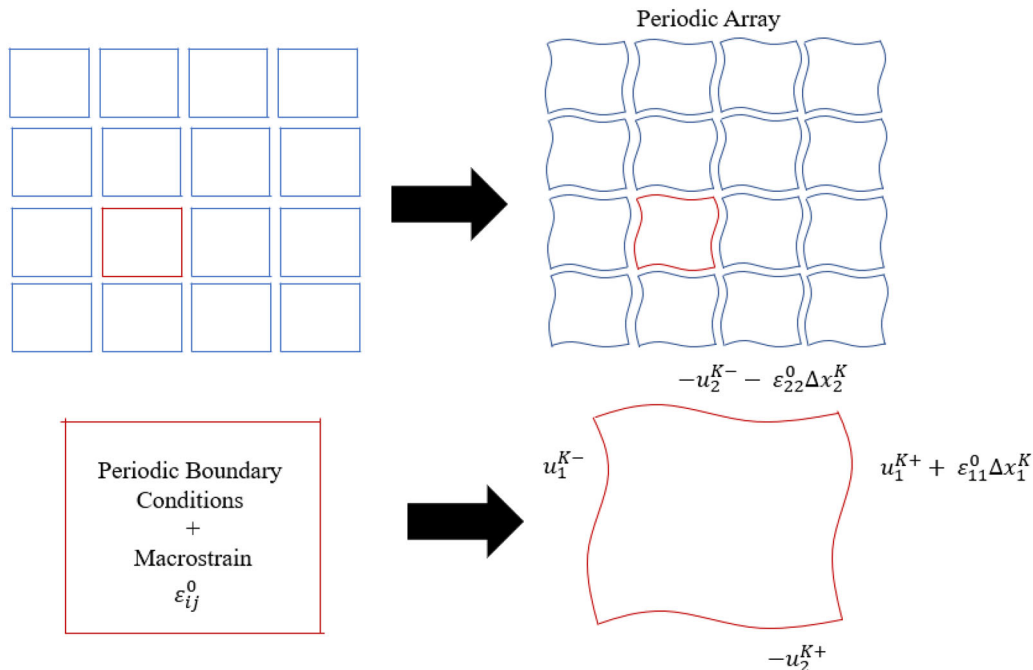

Figure 2. A two-dimensional array under macro strain with periodic boundary conditions [8].

Consider a periodic structure of periodic array under a macroscopic strain.

The displacement field for the structure can be expressed as:

$$u_i(x_1, x_2, x_3) = \varepsilon_{11}^0 x_j + u_i^*(x_1, x_2, x_3) \tag{1}$$

ε_{11}^0 is the macroscopic strain tensor as shown in figure 2. First term on the right side of the equation $(u^0 = \varepsilon_{11}^0 x_j)$ is a linear displacement field, while the second term $u_i^*(x_1, x_2, x_3)$ is a periodic function. Modification of the linear displacement field due to heterogeneity in structure is represented. Displacement must be continuous, i.e., adjacent array cannot be separated or penetrated during deformation. Traction distribution at the opposite parallel boundaries of array must be the same. With this an individual unit cell can be used as a continuous body. For every unit cell boundary surface must appear in parallel pairs. Displacements of parallel opposite surfaces can be written as

$$u_i^{K+} = \varepsilon_{ij}^0 x_j^{K+} + u_i^* \tag{2}$$

$$u_i^{K-} = \varepsilon_{ij}^0 x_j^{K-} + u_i^* \tag{3}$$

Here indices K^+ and K^- identify the Kth pair of the two opposite parallel boundary surfaces of a repeated RVE. $u_i^*(x_1, x_2, x_3)$ is same at the parallel boundaries (periodicity), thus, difference between the two equations is

$$u_i^{K+} - u_i^{K-} = \varepsilon_{ij}^0 \left(x_j^{K+} - x_j^{K-} \right) = \varepsilon_{ij}^0 x_j^K \tag{4}$$

As Δx_j^K are constants for each pair of the parallel boundary surfaces for a specified ε_{ij}^0 the right side of the equation becomes constant. This trick is then used in finite element analysis using displacement constraint equations for implementation of periodic boundary condition. Using above method traction boundary condition is automatically satisfied [8].

Above mentioned approach is extended for Multi-fiber multi-layer representative volume element (M^2RVE) for the cross-ply laminate is shown in figure 1. Hills [25] principle which states that the energy on the micro-level must be the same as the effective energy for the homogenized material over the volume if uniform stresses or strains exist on the boundary of the RVE has been utilized for averaging purpose. In case of M^2RVE elastic modulus is obtained by dividing the volume averaged stress to the volume averaged strain as described in Gibson [2] and elaborated by Sun and Vaidya [26]. More details and implementation of periodic boundary conditions for M^2RVE can be found in [21].

2.3 Loading conditions

To capture the prominent failure mechanisms observed in laminated composites, different loading conditions have been identified. Figure 3 shows various loading conditions used to study micro-scale damage evolution via M^2RVE.
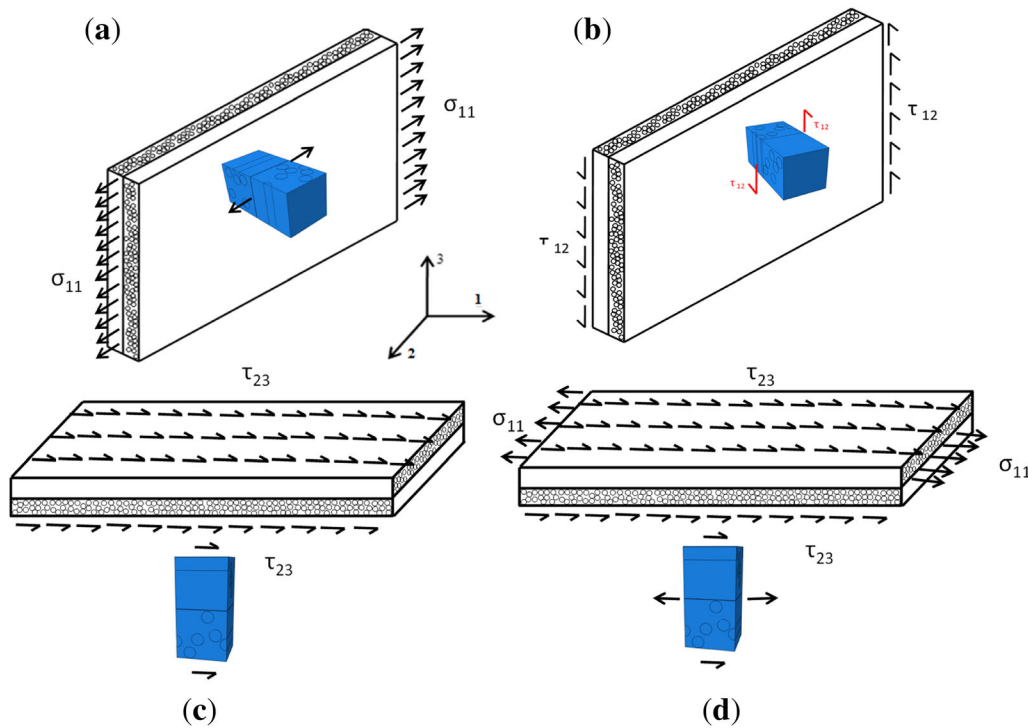

Figure 3. (a) In-plane tensile loading, (b) in-plane shear loading, (c) out-of-plane shear loading and (d) combined in-plane tensile and out-of-plane shear loading.

To capture fiber failure, in-plane tensile loading (see figure 3(a)) has been used. To capture matrix failure and fiber-matrix debonding, in-plane shear loading has been used as shown in figure 3(b). In case of out-of-plane shear loading, interlaminar decohesion (delamination) failure dominates the failure process (see figure 3(c)). To capture all the failure mechanisms simultaneously, in-plane tensile and out-of-plane shear loading have been applied together as illustrated in figure 3(d). A detailed analysis has been performed for each loading condition and global and local damage responses have been characterized.

2.4 *Material properties*

M^2RVE for $[0/90]_n$ laminate has been modeled by using E-glass (ER-459L) fibers having an elastic modulus of 73 GPa and a Poisson's ratio of 0.23. The epoxy matrix (EPOFINE-556 with FINEHARD-951 hardener) has an elastic modulus of 4.7 GPa and a Poisson's ratio of 0.3.

2.5 *Failure criteria*

In the damage process of a laminated composite, different failure mechanisms are involved. However, only one or two of the damage mechanisms drive the failure process for a given loading condition. In case of tensile loading along the fiber direction, fiber failure governs the failure process. Figure 4 shows different failure mechanisms and their respective failure criteria considered during modeling of M^2RVE.

2.5a *Fiber failure* Fibers are the main load-bearing elements of a fiber reinforced composite which means that mechanical properties of the fiber-reinforced composites are governed by fiber strength distribution. Glass fibers typically exhibit a statistical variability in the strength due to the presence of

Figure 4. Schematic representation of the failure criterion used for all the constituents.

randomly distributed flaws which act as stress raisers [27]. 25 E-glass fiber (ER459L) specimens were tested using a computer-controlled universal testing machine (*Favigraph*, *Textechno*), in order to measure their tensile strengths. All the tests were performed in a displacement control mode at a rate of 2 mm/min and at ambient temperature and pressure. All samples were maintained under load until mechanical failure occurred, with failure being defined as the point in which the glass fiber no longer supported the externally applied load. Tensile strength was taken as the ratio of the maximum load applied to the cross-sectional area of the specimen. All the precautions about material, specimen preparation, specimen conditioning, environment of testing, specimen alignment and gripping, speed of testing are taken to ensure additional flaws are not introduced into the glass fibres during testing.

It is explicitly mentioned in the literature that the failure strength of the brittle material varies a lot and it is difficult to determine the strength value to be used for modeling of brittle materials. Weibull distributions [28, 29] have been widely used to predict the appropriate tensile strength of the glass fibers from experimental findings. The two-parameter Weibull distribution for prediction of tensile strength of the glass fibers can be expressed as follows [30]:

$$P(\sigma) = 1 - e^{\left(\frac{\sigma}{\sigma_0}\right)^m} \tag{7}$$

where $P(\sigma)$, in the range of [0, 1], is the failure probability of single fiber under an applied stress less than or equal to σ. σ_o is a characteristic value of stress σ at which 63% of the population of specimens has failed (also known as *alpha(α)* - characteristic life). m is the Weibull modulus which describes the variability in the failure strengths. The common values for 'm' of fibers range from 2 to 20 [31]. A high Weibull modulus is desirable as it indicates better predictable failure behavior. The stress, σ, is simply obtained from the experimental results, while there are several probability estimators, also known as ranking methods, available in the literature [32]. The most common probability estimators for brittle failure with small sample size can all be written in the form [33]:

$$P = \frac{i - 0.5}{n} \tag{8}$$

where i denotes that it is the ith, specimen in the lot, while n represents the sample size. Taking the natural log on the both sides of the Equation (8), results in:

$$Y_i = In\left(In\left\{\frac{1}{1 - P(\sigma)}\right\}\right) \tag{9}$$

$$X_i = In(\sigma_i) \tag{10}$$

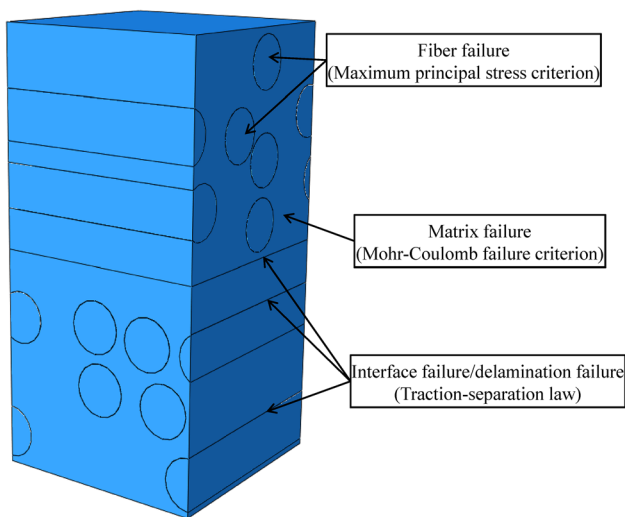$$C = -mIn(\sigma_0) \tag{11}$$

$$Y_i = mX_i + C \tag{12}$$

As shown in Equation (12), the Weibull distribution function can be linearized. A linear plot between X_i and Y_i, is termed as Weibull probability plot (WPP). If the correlation coefficient of the plot is closed to 1, the strength distribution can use the two parameter Weibull distribution function. Figures 5(a) and (b) show WPP and Weibull plot, respectively. The correlation coefficient is 0.9, which is close to 1 as required. Figure 5(b) is used for estimating parameters m and C.

The values of parameters are determined as $m=6.217$ and $\sigma_0=1745.85$ MPa from the data given in figure 5.

The Weibull distribution has an expected value (or mean value) of tensile strength is given by [30]:

$$\sigma_m = \sigma_0 \Gamma \left(1 + \frac{1}{m}\right) \qquad (13)$$

where Γ is the gamma function.

Substituting parameters m, σ_0 in Equation (13), the mean value of the tensile strength is found to be 1623.3 MPa. The mean measured tensile strength of the glass fiber is 1621 MPa which is close to the value obtained from the Weibull distribution. The maximum principal stress failure criterion has been conventionally used to capture the failure of brittle materials [27]. Therefore, the maximum principal stress criterion is used for modeling the failure of glass fibers.

2.5b *Matrix failure* The epoxy matrix (EPOFINE-556) has been assumed to behave as an isotropic, elastic-plastic solid following the Mohr-Coulomb yield criterion [24]. The Mohr-Coulomb criterion given in Equation (14) assumes that the yielding takes place when the shear stress, τ, acting on a specific plane reaches a critical value, which depends on normal stress, σ_n, acting on that plane. This criterion incorporates the effect of tri-axiality on the yielding under shear stress. The corresponding yield surface is expressed in terms of the maximum and minimum principal stresses (σ_I and σ_{III}) in Equation (15).

Figure 6. Standard traction-separation law [4].

$$|\tau| = c - \sigma_n \tan \varphi \qquad (14)$$

$$F(\sigma_I, \sigma_{III}) = (\sigma_I - \sigma_{III}) + (\sigma_I + \sigma_{III}) \sin \varphi - 2c \cos \varphi = 0 \qquad (15)$$

where c is the flow stress of epoxy matrix under pure shear and φ stand for the epoxy matrix friction angle that accounts for the effect of tri-axiality. The values of c and φ are determined as 37.7 MPa and 15°, respectively, by using tensile and compressive strength of the matrix material. Details about the implementation of Mohr-Coulomb criterion can be found in Soni *et al* [21].

2.5c *Fiber-matrix interface failure* The progressive fiber-matrix interfacial decohesion has been simulated using standard cohesive surface elements in ABAQUS Standard® as shown in figure 6 [4]. The mechanical behavior of the interface has been modeled using a traction-separation law which correlates the displacement across the interface with
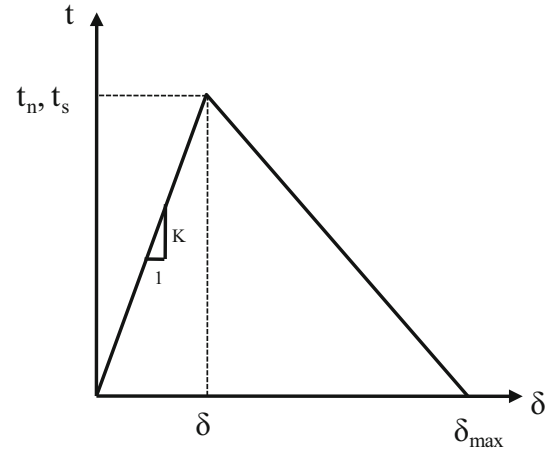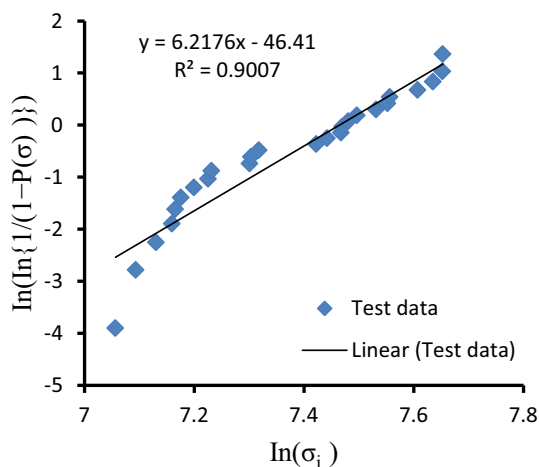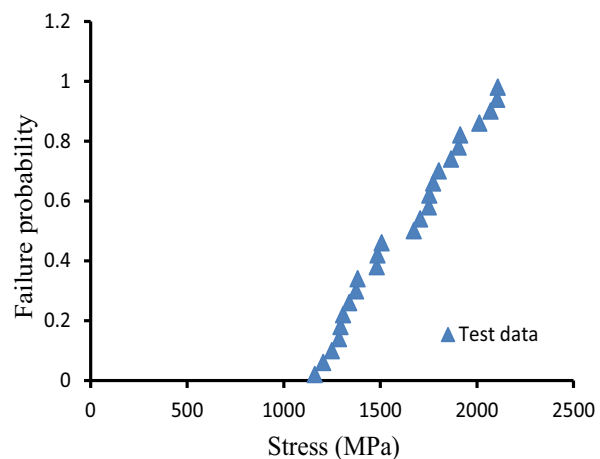

Figure 5. (a) WPP for tensile strength of the glass fibers. (b) Weibull plot.

the force vector acting on it. Without any damage, the interface behavior is assumed to be linear with very high initial stiffness (K=35 GPa) for maintaining the displacement continuity at the interface.

The linear behavior ends at the onset of damage which can be expressed as follows for maximum stress criteria:

$$\max \left\{ \frac{t_n}{N}, \frac{t_s}{S} \right\} = 1 \qquad (16)$$

where t_n and t_s are normal and tangential stresses transferred by the interface, respectively. t_n is either positive or zero because compressive normal stresses do not cause the opening of the crack. N and S are the normal and tangential interfacial strengths, respectively, assumed to be equal in this work. Equation (16) is generalized elaboration of tractions separation law. A default tolerance of 1% has been used for normal and tangential stresses.

In all the simulations in previous studies by Soni *et al* [21] as well in this study maximum deformation observed is less than 4%, hence it can be said that traction-separation assumption is consistent with small deformation assumption.

In addition to the cohesive strength (N, S), the fracture energy, $\acute{\Gamma}$, also governs the interface behavior. The energy consumed during the fracture of the interface is considered to be independent of the loading path in the interface failure model. Fracture energy, Γ, is given by:

$$\Gamma = \frac{1}{2} t \Delta \delta \qquad (17)$$

where t (t_n or t_s) is the cohesive strength of the interface and 'δ' is the displacement across the interface. Zhou *et al* [34] conducted various experiments on determining interfacial strength and fracture energy (Gamma). It has been found that interfacial strength values lie between 24 MPa and 38 MPa by fragmentation testing and 28 MPa and 58 MPa by a push-out test for the same glass fiber/epoxy composite system. There is a variation of as much as 6 times in some cases in the values estimated using these two methods. The measurement of the interface properties involves complex and costly experiments which yield substantial variation in the results. To address this issue, various values of interfacial strengths and fracture energy have been used in accordance with experimental results in Soni *et al* [21]. The realistic value of interfacial strength Γ=100 J/m^2 is assumed in the current work, in accordance with value suggested by Zhou *et al* [33].

2.5d *Delamination between plies failure* The progressive delamination between plies has been simulated by using the traction-separation law with cohesive (COH3D6) elements. In the absence of any damage, the interface behavior is assumed to be linear with an initial stiffness equal to the stiffness of the matrix material, i.e., 4.7 GPa because in case of cross ply laminate fiber bridging effect can be

neglected [25]. A fracture energy of 100 J/m^2 has been kept constant throughout the simulations [34]. Damage initiation has been captured using quadratic nominal stress criterion expressed as [5]:

$$\left\{ \frac{t_n}{t_n^0} \right\}^2 + \left\{ \frac{t_s}{t_s^0} \right\}^2 + \left\{ \frac{t_t}{t_t^0} \right\}^2 = 1 \qquad (18)$$

where t_n, t_s and t_t are normal and tangential stress in one direction and tangential stress in another direction respectively. t_n is considered as positive all the time, as compressive stress does not cause the opening of the crack. t_n^0, t_s^0 and t_t^0 are normal and tangential strength in one direction and tangential another direction respectively. The adhesive strength of the delamination is varied above and below 30 MPa (close to the measured shear strength of the matrix material) to study its effect on overall material response. Equation (18) has been used for implementation of traction separation law in the simulations.

3. Experimental work (in-plane tensile loading)

Experimental data was not available in the literature for the epoxy/fiber combination used in the model; therefore, experiments were conducted on glass fiber-epoxy laminate specimens. [0/90] E-glass fiber/epoxy matrix laminates were manufactured using a hand lay-up technique. The fiber volume fraction (V_f) was found to be equal to 28%, determined experimentally, according to ASTM D2584 (ASTM D2584–11, 2000) [35]. The edges of the laminate were removed and rectangular specimens (25×250 mm^2) were cut from the [0/90] laminate according to ASTM standard D3039 (D3039/D3039M–08, 2008) [29] as shown in figure 7. A calibrated electronic strain indicator was used to note the strain developed in the strain gauge during the loading of the specimen.

In-plane tensile strength tests were performed for the E-glass/epoxy [0/90] laminates as per ASTM 3039 (ASTM D3039/D3039M–08, 2008) [36]. The specimens were tested in tension using a *LS 100 plus* universal testing machine by *LLOYD* instruments under stroke control and at a constant cross-head speed of 1 mm/min. The applied load was measured simultaneously with a 100 kN load cell. The corresponding tensile strain, ε_{11}, was noted using a strain gauge mounted on the specimen. The in-plane tensile stress-strain curve, up to 2.5% strain, is plotted in figure 8 (a) for [0/90] laminates.

4. Global stress-strain response for in-plane tensile loading

The FE analysis has been performed using Rik's algorithm for nonlinear analysis in ABAQUS Standard®[4]. Rik's algorithm is a type of 'arc length' method used for solving
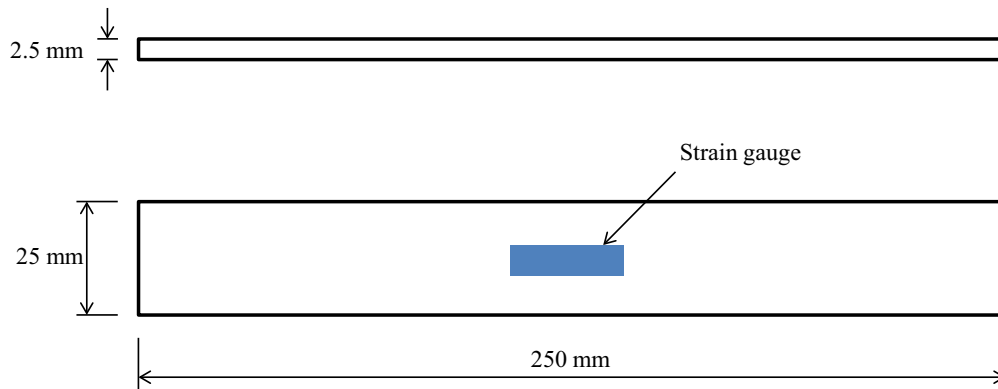
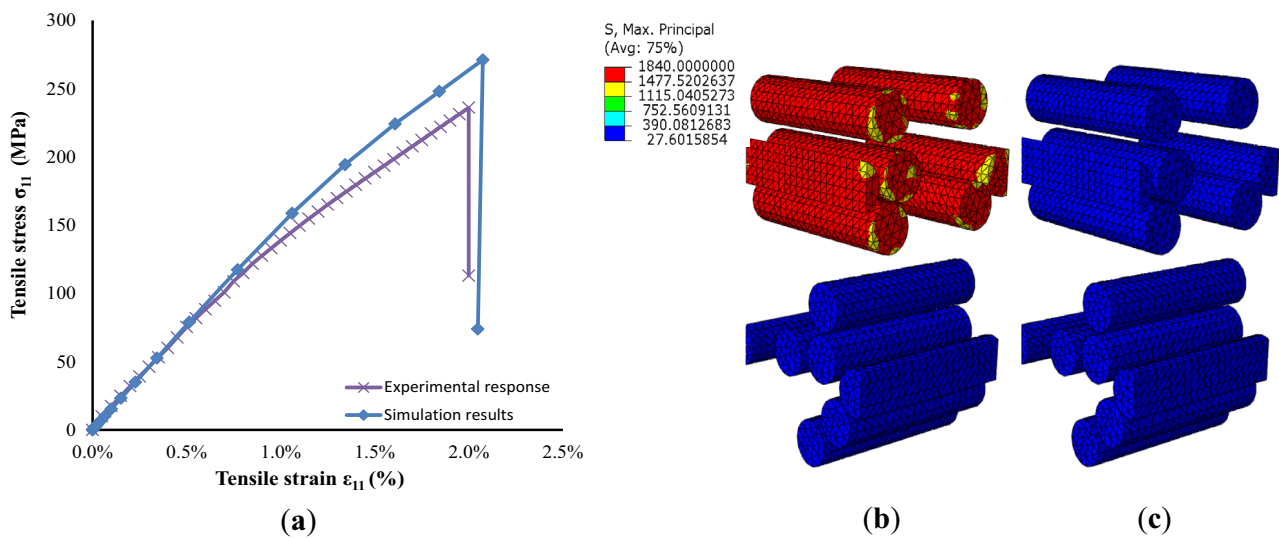**Figure 7.** Specimen dimensions in-plane tensile loading tests.

Figure 8. (a) In-plane tensile stress-strain response of M²RVE for [0/90]ₙ laminate. (b) Maximum principal stress in the E-glass fibers before fiber failure. (c) Maximum principal stress in the E-glass fibers after fiber failure.

complex nonlinear problems [4, 37]. At the end of each load step in the non-linear analysis, volume average stresses and strains for the $[0/90]_n$ laminate have been plotted along with the experimental response, as shown in figure 8 (a).

The initial region of the stress-strain curve perfectly matches with the experimental results up to a tensile strain of approximately 0.5%. Beyond this point, the simulation results overpredict the stresses as compared to the experimental response. The failure strength predicted by the simulation was 14% higher than the failure strength determined experimentally. This error may be attributed to a stiffer matrix in the experimental specimen as compared to the FE simulation. Another plausible explanation can be automated incremental checking of the fiber failure criterion in the finite element code so some of the fiber failure is detected in the subsequent time step which can result in higher stress values. Each fiber was assigned a strength value between 1100 MPa and 1800 MPa. When the

maximum principal stress in the fiber material reaches the limiting value, the stiffness of the element has been reduced significantly (>90%) which mimics the fiber failure. The stiffness value is not reduced to zero in order to avoid the stress singularity. However, as soon as the minimum strength is reached in any element (1100 MPa in the present case), the strength of the entire RVE reduces significantly and the remaining fibers fail within a single step. Hence, a random distribution of the strength is not advisable as it will trigger failure close to the lowest value. Consequently, the mean value of the fiber strength obtained from the Weibull distribution has been used instead. When the maximum principal stress in any element in the fiber material is greater than 1623 MPa then the element is considered to have failed and the stiffness of the particular element is reduced significantly (>90%). Failure strain predicted by simulation is almost equal to the failure strain predicted by experiments. Fiber-matrix interfacial properties are kept as stiffness=35 GPa/m, strength=30 MPa and

Fracture energy=100 J/m^2. Delamination layer material properties are strength=30 MPa, stiffness=4.7 GPa (the same as the matrix material) and fracture energy=100 J/m^2. To address the sensitivity of these properties, the effect of these parameters on the material response has been characterized later in the paper.

5. Study of damage evolution mechanisms

As explained previously, the aim of the paper is to demonstrate capability of M^{2}RVE to capture all the possible damage mechanisms in composite laminates. Therefore, the damage evolution studies have been conducted for different scenarios are shown in figure 3.

5.1 *Tensile failure dominated damage mechanism*

It is known that in-plane tensile loading leads to a fiber failure. To simulate in-plane tensile loading, M^{2}RVE is subjected to displacement in direction 1 as shown in figure 3(a). To capture fiber failure, a Fortran® based user subroutine "USDFLD" has been used. The maximum principal stress developed in each element of the E-glass fiber material is called by using another user subroutine "GETVRM". The stress developed in each element of the E-glass fiber material is then compared with the average failure stress obtained from a Weibull distribution plot (1623 MPa) to detect the fiber failure. The top and bottom lamina of M^{2}VE are referred to as 0° (along the applied displacement) and 90° (perpendicular to the applied displacement), respectively. It can be observed in figure 8 (b) that all the fibers in 0° lamina have failed where the loading is in-line with the fiber if the applied stress exceeded 1623 MPa. As shown in figure 8(a), the M^{2}RVE also captures the global stress-strain response with reasonable accuracy. Figures 8(b) and (c) show the contours of the maximum principal stresses that developed in fibers prior to the onset of failure and post failure, respectively. It must be noted that all the experiments are conducted on [0/90]$_n$ composites lay-up

To study the effect matrix properties on the global response, the matrix fraction angle is varied between 5° and 15°. Consequently, the cohesive strength of the matrix is varied between 41 MPa and 48.8 MPa. It has been observed that there is no effect of the change in matrix properties on the global stress strain response. Similarly, in order to study the effect of fiber-matrix interfacial and interlaminar properties, a parametric study has been performed. The cohesive strength of the interfacial material has been varied from 5 MPa to 90 MPa while the stiffness of the cohesive layer has been kept as 35 GPa/m. It has been found that there is no effect of the interfacial strength on the global stress strain response. It has also been found that there is no effect of the properties of the delamination layer between

the two laminae on the global stress strain response for in-plane tensile loading. Based on these results, it can be inferred that fiber failure is the dominant mechanism and other modes of failures are inappreciable.

5.2 *Matrix and interface dominated failure mechanism*

In order to study matrix damage and fiber-matrix interfacial failure simultaneously, an in-plane shear loading has been applied as shown in figure 3(b). The M^{2}RVE has been subjected to a 4% shear strain, since the experimental results are available up to 4% shear stain [21]. The maximum principal stresses developed in the E-glass fibers at a 4% shear strain is much lesser than 1623 MPa, therefore, no element in the fiber experiences failure which indicates that fiber failure can be ignored in in-plane shear loading. The mean of the maximum principal stresses is about ~300 MPa which indicates that fiber failure can be ignored in in-plane shear loading.

It has already been demonstrated by Soni *et al* [21] that the matrix material properties affect the global stress strain response. Figure 9 (a) shows the volume averaged in-plane shear stress-strain response of the M^{2}RVE along with the experimental response. It can be observed that simulated response is in good agreement with the experimental response. The matrix friction angle is varied between 5° and 15° in increments of 5° as shown in figure 8 (a). It can be observed that with an increase in the friction angle and, therefore the matrix cohesive strength, there is an increase of ~17% in shear stresses if the friction angle in increased from 5° to 15° .

It can be observed in figure 9 (b) that the global response gets significantly affected by the interface properties as well. The shear strength of the material for an interfacial strength of 5 MPa is ~36% lower than the shear strength for the material with an interfacial strength of 30 MPa. However, any further increase in the interfacial strength does not affect the global shear stress-strain response.

QUADSCRT is a damage initiation criterion for cohesive elements. Similar to the tensile loading, the onset of interlaminar decohesion does not occur, however, the magnitude of "QUADSCRT" is higher for in-plane shear loading as compared to the tensile loading indicating that the interlaminar traction is higher for in-plane shear. Since, decohesion does initiate, the effect of delamination on the global stress-strain response is negligible.

5.3 *Interfacial and interlaminar decohesion driven failure mechanism*

The previous two conditions do not exhibit any sensitivity to the interlaminar decohesion (delamination). To demonstrate interfacial failure between fiber-matrix and
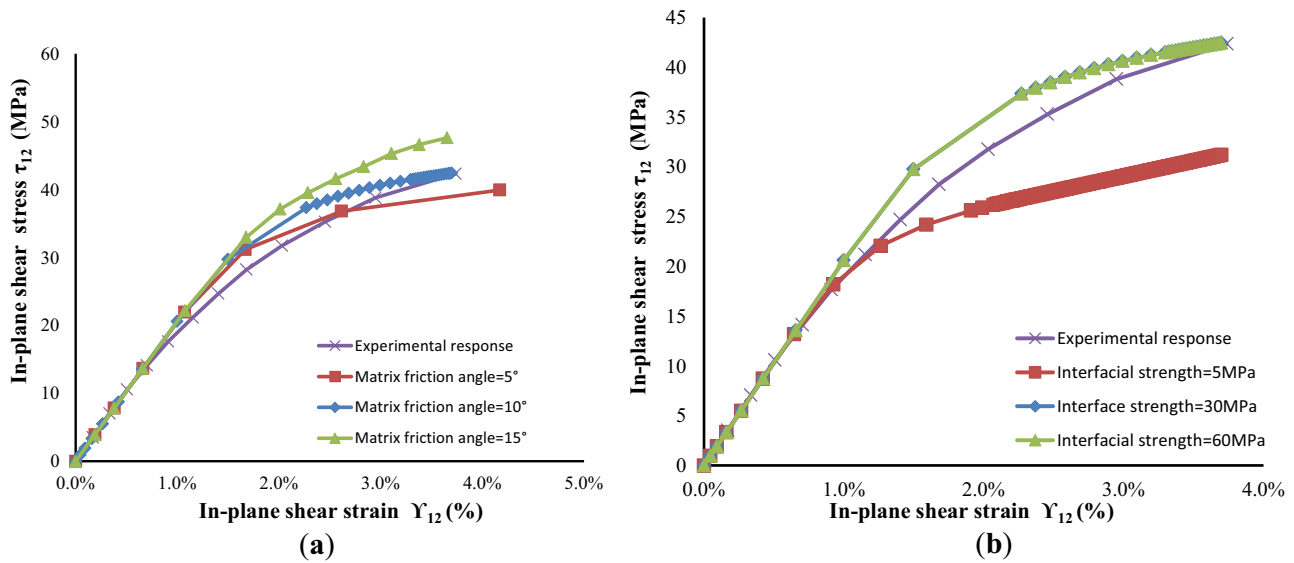
Figure 9. Stress-strain response of M²RVE for [0/90]ₙₛ laminate subjected to in-plane shear loading. (a) Effect of matrix friction angle. (b) Effect of fiber-matrix interfacial properties.

delamination between layers, out-of-plane shear loading has been applied as shown in figure 3(c). M²RVE has been found to be reasonably accurate for different loading conditions; it is expected that it can capture the response of complex loading conditions which are difficult to realize such as out-of-plane shear loading.

The interfacial strength and stiffness have been kept as 30 MPa and 35 GPa/m, respectively (as used in case of in-plane tensile loading and in-plane shear loading). Delamination layer strength and stiffness have been kept as 30 MPa and 4.7 GPa/m, respectively. The material response obtained from the above-mentioned parameters has been used as a baseline for comparing the parameter sensitivity. It is expected that the fiber failure is unlikely to occur in this type of loading where fibers will not be experiencing tension. The maximum principal stresses are much below (<1000 MPa) the fiber failure limit of 1623 MPa. In addition, the effect of the matrix damage parameters has not been found to be significant on the out-of-plane shear stress-strain response.

The strength of the interfacial layer is varied from 5 MPa to 60 MPa, keeping the stiffness of the interfacial layer as 4.7 GPa. Figure 10 (a) shows that the effect of the interfacial strength on the material response is significant and the out-of-plane shear stresses have increased by 28% if the interfacial strength increased from 5 MPa to 30 MPa. Any additional increase does not improve the material response.

To study delamination between 0° ply and 90° ply, the strength of the delamination layer is varied from 5 MPa to 90 MPa keeping stiffness equal to 4.7 GPa. It is observed that the complete failure of the cohesive elements in the delamination layer occurs at 1.5% out-of-plane shear strain when delamination layer strength of 5 MPa which does not change appreciably till 30 MPa. However, if the strength of

the delamination layer is increased to 90 MPa, the delamination failure takes place at ∼3.2% out-of-plane shear strain as shown in figure 10 (b).

The contour plot of variable "QUADSCRT" in figure 11 (a) shows that, if the delamination layer strength is equal to 5 MPa, the complete damage in the delamination layer takes place and value of QUADSCRT reaches 1. However, if the delamination layer strength equals 90 MPa, the maximum value of the damage parameter is limited 0.201 as shown in figure 11 (b).

5.4 *Combined failure driven by fiber damage, fiber-matrix debonding and interlaminar decohesion*

To demonstrate the capability of the M²RVE to capture multiple (more than two) failure mechanisms simultaneously, a multi-axial complex loading shown in figure 3 (d) has been applied. It is a combination of in-plane tensile loading and out-of-plane shear loading. The applied displacement in the case of in-plane tensile loading and out-of-plane shear loading has been maintained at a ratio of 1:12 ($\delta_t/\delta_s = 1/12$) to avoid predominant tensile failure.

Figures 12(a) and (b) show the contour plot of the principal stresses developed in the E-glass fibers. In this case, the fibers in the 0° lamina take the entire load and it can be observed that the stresses in the fibers reduced drastically after fiber failure criteria was reached, as shown in figure 12 (b).

To study the effect of complex loading on epoxy matrix damage, the matrix friction angle has been varied between 5° and 15°, as shown in figure 12 (c). It can be observed that the failure of the composite occurs at 0.6% tensile
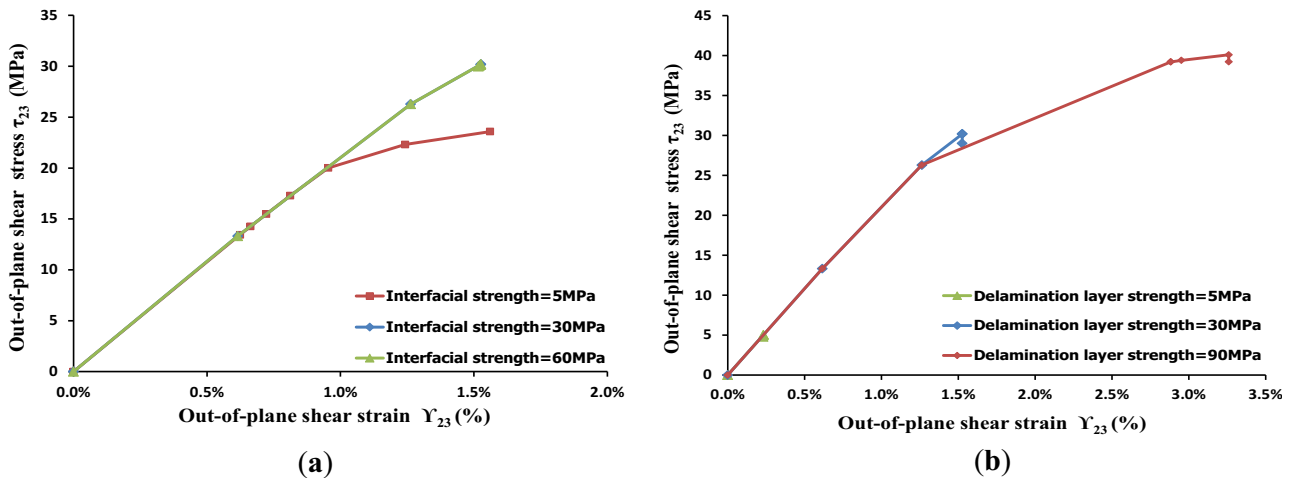
Figure 10. (a) Effect of fiber-matrix interfacial properties on the stress-strain response of M^{2}RVE for [0/90]$_n$ laminate. (b) Effect of delamination layer properties on the stress-strain response of M^{2}RVE for [0/90]$_{ns}$ laminate subjected to out-of-plane shear loading.

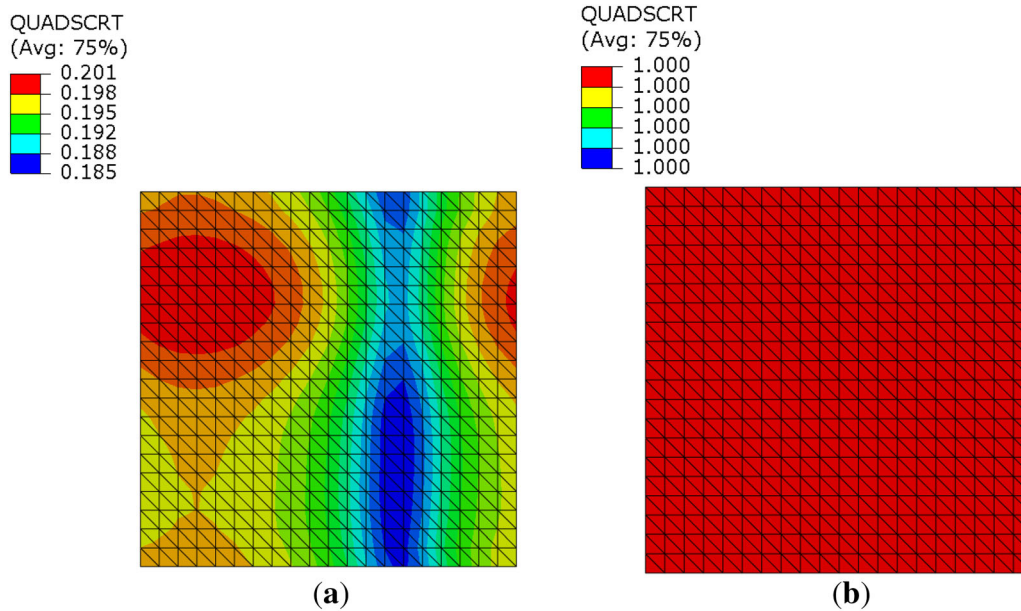**Figure 11.** QUADSCRT for delamination layer strength: (a) 90 MPa; (b) 5 MPa at 1.5% out-of-plane shear strain.

strain, which is ∼70% less than the failure strain obtained under pure in-plane tensile loading. The tensile stress at fiber failure is ∼105 MPa which is ∼60% lower than the tensile strength obtained in pure in-plane tensile loading. In case of out-of-plane shear loading response, failure strain has been ∼1.5%, which is same as in case of pure out-of-plane shear loading. The shear stress at the failure is also same as that obtained in pure out-of-plane shear loading. Unlike pure out-of-plane shear response, there is no discernible variation in the shear response when combined loading has been used for different matrix friction angles, as shown in figure 12 (c). Figure 13 (a) shows the material response in case of combined loading for different

interfacial material properties. It can be observed that there is no effect of the variation of interfacial properties on fiber failure. However, out-of-plane shear strength is lower if the interfacial strength is less than 30 MPa.

To study the effect of the interlaminar properties on the material response, the strength of the delamination layer (interlaminar cohesive strength) is varied between 5 MPa and 60 MPa, keeping the stiffness at 4.7 GPa as shown in figure 13 (b). It is observed that there is no effect of this change on the fiber failure, however, the composite failure takes place at a much lower stress and strain (5 MPa and 0.2%) for the interlaminar cohesive strength of 5 MPa. Figure 13 (b) shows that the failure occurs at 30 MPa and
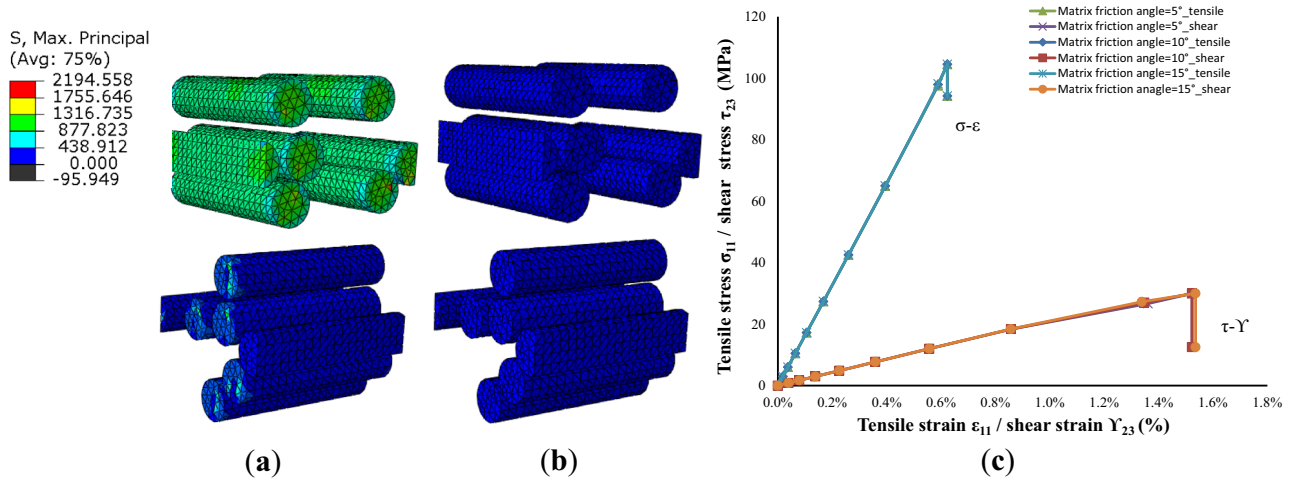
Figure 12. Maximum principal stress in the E-glass fibers at 0.6% of in-plane tensile strain and at 1.5% out-of-plane shear strain (a) before fiber failure; (b) after fiber failure; (c) effect of matrix shear angle on material response.
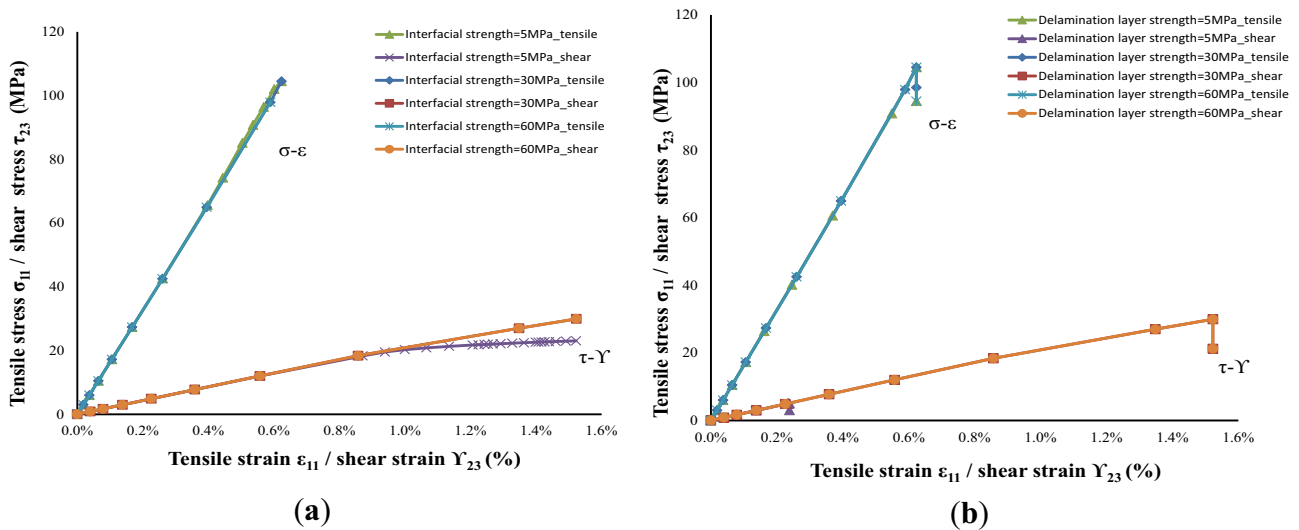

Figure 13. (a) Effect of fiber-matrix interfacial properties on the stress-strain response of the M²RVE for the [0/90]ₙₛ laminate subjected combined loading; (b) effect of delamination layer properties on the stress-strain response of the M²RVE for the [0/90]ₙₛ laminate subjected combined loading.

1.5% shear strain under pure out-of-plane shear loading for a delamination layer strength of 5 MPa. In comparison, under combined loading with same interlaminar cohesive strength, the failure occurs at a substantially lower out-of-plane stress and strain values as shown in figure 13 (b).

In the previous work by Soni *et al* [21] as well as in the present study, it has been observed that the results are mainly functions of material properties of fibers and matrix, fibermatrix interface properties and inter-layer properties. Therefore, it can be said that the simulation response observed in the present study may remain the same for higher volume fractions of the fibers.

6. Conclusions

The work has presented a use of multi-layer multi-fiber representative volume element (M²RVE) to predict global stress-strain material response for various failure mechanisms operating under simple and multi-axial loading. The results show that this strategy has been able to reproduce, accurately, the physical behavior which has been observed experimentally. The model has the potential to reproduce very complex stress states and the ability to carry out systematic parametric studies to optimize composite properties. The following specific conclusions can be drawn from the current work.

- M^{2}RVE can be used to capture all the failure modes, viz, fiber failure, matrix cracking, fiber-matrix debonding and the delamination between plies in a periodic media. Fiber failure dominates all other failure mechanisms when fibers have been subjected to tensile loading.

- In case of 0.6% of in-plane tensile strain and at 1.5% out-of-plane shear, the fiber failure occurs at much lower global stresses ($\sim$60% lower) which can be observed from figure 12 (c).

- The fiber-matrix interface properties affect the material response under in-plane shear loading. However, under combined out-of-plane shear and tensile loading the effect of fiber-matrix interface properties is not as pronounced as the interlaminar properties.

- Composite failure occurs at much lower stress and strain values (5 MPa and 0.2%) for a relatively low interlaminar strength of 5 MPa under combined in-plane tensile and out-of-plane shear loading. Hence, it can be inferred that the interlaminar properties play a significant role in the global material response in complex multi-axial loading.

7. List of symbols

ε	Macroscopic Strain Tensor
σ	Applied Stress
K	Stiffness
V_f	Fiber volume fraction
σ_n	Normal Stress
$P(\sigma)$	Failure Probability of Single Fiber
$alpha(\alpha)$	Characteristic Life
m	Weibull Modulus
Γ	Gamma Function
c	Flow Stress of Matrix under Pure Shear
φ	Matrix Friction Angle
t_n	Normal Stresses at Interfaces
t_n	Tangential Stresses at Interfaces
N	Normal Interfacial Strengths
S	Tangential Interfacial Strengths
$\acute{\Gamma}$	Fracture energy
δ	Displacement across the Interface
QUADSCRT	Damage Initiation Criterion for Cohesive Elements

References

[1] Gibson R F 2016 *Principles of composite material mechanics*, fourth edition, CRC Press Taylor & Francis Group, Chapter 10: Mechanical Testing of Composites and Their Constituents, pages 569–630

[2] Kanoute P, Boso D P, Chaboche J L and Schrefler B A 2009 Multiscale methods for composites: A review. *Arch. Comput. Meth. Eng.* 16: 31–75

[3] Feyel F 2003 A multilevel finite element method (FE^2) to describe the response of highly non-linear structures using generalized continua. *Comput. Methods Appl. Mech. Eng.* 192: 3233–3244

[4] Abaqus 2018 User's manual, ABAQUS, Inc.

[5] Wang A S D and Yan K C 2005 On modeling matrix failures in composites. *Composites Part A.* 36: 1335–1346

[6] Soni G, Gupta S, Singh R, Mitra M, Yan W and Falzon BG 2014 Study of localized damage in composite laminates using micro-macro approach. *Compos. Struct.* 113: 1–11

[7] Berger H, Kari S, Gabbert U, Rodriguez-Ramos R, Bravo-Castillero J and Guinovart-Diaz R A 2005 Comprehensive numerical homogenization technique for calculating effective coefficients of uniaxial piezoelectric fibre composites. *Mater. Sci. Eng. A.* 412: 53–60

[8] Kassem G A 2009 *Micromechanical material models for polymer composites through advanced numerical simulation techniques*. Ph.D. thesis. RWTH University, Aachen, North Rhine-Westphalia, Germany

[9] Totry E, González C and LLorca J 2008 Failure locus of fiber-reinforced composites under transverse compression and out-of-plane shear. *Compos. Sci. Technol.* 68: 829–839

[10] Totry E, Molina-Aldareguia J M, González C and LLorca J 2010 Effect of fibre, matrix and interface properties on the in-plane shear deformation of carbon-fibre reinforced composites. *Compos. Sci. Technol.* 70: 970–980

[11] Xia Z, Chen Y and Ellyin F 2000 A meso/micro-mechanical model for damage progression in glass-fibre/epoxy cross-ply laminates by finite-element analysis. *Compos. Sci. Technol.* 60: 1171–1179

[12] González C and LLorca J 2006 Multiscale modeling of fracture in fiber-reinforced composites. *Acta Mater.* 54: 4171–4181

[13] Wang H, Qin Q, Ji H and Sun Y 2011 Comparison among different modeling techniques of 3D micromechanical modeling of damage in unidirectional composites. *Adv. Sci. Lett.* 4: 400–407

[14] Cox B, Bale H, Begley M, Blacklock M, Do B, Fast T, Naderi M, Novak M, Rajan V, Rinaldi R, Ritchie R, Rossol M, Shaw J, Sudre O, Yang Q, Zok F, Marshall D 2014 Stochastic virtual tests for high-temperature ceramic matrix composites. *Annual Rev. Mater. Res.* 44: 479–529

[15] Pulungan D, Lubineau G, Yudhanto A, Yaldiz R, Schijve W 2017 Identifying design parameters controlling damage behaviors of continuous fiber-reinforced thermoplastic composites using micromechanics as a virtual testing tool. *Int. J. Solids Struct.* 117: 177–190

[16] Madadi H R and Farrokhabadi, A 2018 Development a refined numerical model for evaluating the matrix cracking and induced delamination formation in cross-ply composite laminates. *Compos. Struct.* 200: 12–24

[17] Ahmadian H, Yang M, Nagarajan A, Soghrati S 2019 Effects of shape and misalignment of fibers on the failure response of carbon fiber reinforced polymers. *Comput. Mech.* 63: 999–1017

[18] Ramdoum S, Fekirini H, Bouafia F, Benbarek S, Serier B, Feo L 2018 Carbone/epoxy interface debond growth using

the Contour Integral/Cohesive zone method. *Compos. Part B- Eng.* 142: 102–107

[19] Romanowicz M 2019 Micromechanics-based prediction of the failure locus of angle-ply laminates subjected to biaxial loading. *J. Compos.* 53: 3577–3587

[20] Bargmann S, Klusemann B, Markmann J, Schnabel J, Schneider K, Soyarslan C, Wilmers J 2018 Generation of 3D representative volume elements for heterogeneous materials: A review. *Prog. Mater. Sci.* 96: 322–384

[21] Soni G, Singh R, Mitra M and Falzon B G 2014 Modeling matrix damage and fibre-matrix interfacial decohesion in composite laminates via a multi-fibre multi-layer representative volume element (M^2RVE). *Int. J. Solids Struct.* 51: 449–461

[22] Ullah Z, Kaczmarczyk L, Pearce C J 2017 Three-dimensional nonlinear micro/meso-mechanical response of the fibre-reinforced polymer composites. *Compos. Struct.* 161: 204–214

[23] Matsuda T, Okumura D, Ohno N and Kawai M 2007 Three-dimensional microscopic interlaminar analysis of cross-ply laminates based on a homogenization theory. *Int. J. Solids Struct.* 44: 8274–8284

[24] Digimat 2018 Users' manual, DIGIMAT, Inc.

[25] Hill, R 1963 Elastic properties of reinforced solids: some theoretical principles. *J. Mech. Phys. Solids* 11: 357–372

[26] Sun, C T, Vaidya, R S 1996 Prediction of composite properties from a representative volume element. *Compos. Sci. Technol.* 56: 171–179

[27] Feih S, Tharaner A and Lilholt H 2005 Tensile strength and fracture surface characterization of sized and unsized glass fibers. *Mater. Sci.* 40: 1615–1623

[28] Shao J, Wang F, Li L and Zhang J 2013 Scaling Analysis of the Tensile Strength of Bamboo Fibers Using Weibull Statistics. *Adv Mater Sci Eng.* Article ID 167823

[29] Weibull WA 1951 Statistical distribution function of wide applicability. *J. Appl. Mech.* 293–297

[30] Hao W, Melkote S and Danyluk S 2012 Mechanical Strength of Silicon Wafers Cut by Loose Abrasive Slurry and Fixed Abrasive Diamond Wire Sawing. *Adv. Eng. Mater.* 14: 342–348

[31] Mahesh S, Beyerlein I and Phoenix S 1999 Size and heterogeneity effects on the strength of fibrous composites. *Physica D.* 133: 371–389

[32] Standard practice for reporting uniaxial strength data and estimating Weibull distribution parameters for advanced ceramic 2013 ASTM Standard C1239-13, Philadelphia, PA, USA

[33] Bergman B 1984 On the estimation of the Weibull modulus. *J. Mater. Sci. Lett.* 3: 689–692

[34] Zhou XF, Wagner H D and Nutt SR 2001 Interfacial properties of polymer composites measured by push-out and fragmentation tests. *Composites Part A.* 32: 1543–1551

[35] Standard Test Method for Ignition Loss of Cured Reinforced Resins 2000 ASTM Standard D2584-11. West Conshohocken, PA, https://doi.org/10.1520/d2584-11, USA

[36] Standard test method for tensile properties of polymer matrix composite materials 2008 ASTM Standard D3039/D3039M. West Conshohocken, PA, https://doi.org/10.1520/d3039_d3039m-08, USA

[37] Riks E 1979 An incremental approach to the solution of snapping and buckling problems. *Int. J. Solids Struct.* 15: 529–551